JBC ARTICLE

Solution structure and flexibility of the condensin HEAT-repeat subunit Ycg1

Received for publication, March 29, 2019, and in revised form, July 24, 2019 Published, Papers in Press, July 26, 2019, DOI 10.1074/jbc.RA119.008661

Karen Manalastas-Cantos[‡1], Marc Kschonsak[§2], Christian H. Haering[§], and Dmitri I. Svergun[‡3]

From the [‡]European Molecular Biology Laboratory, Hamburg Unit, Hamburg 22607, Germany and the [§]European Molecular Biology Laboratory, Heidelberg 69117, Germany

Edited by Karen G. Fleming

High-resolution structural analysis of flexible proteins is frequently challenging and requires the synergistic application of different experimental techniques. For these proteins, small-angle X-ray scattering (SAXS) allows for a quantitative assessment and modeling of potentially flexible and heterogeneous structural states. Here, we report SAXS characterization of the condensin HEAT-repeat subunit Ycg1^{Cnd3} in solution, complementing currently available high-resolution crystallographic models. We show that the free Ycg1 subunit is flexible in solution but becomes considerably more rigid when bound to its kleisin-binding partner protein Brn1^{Cnd2}. The analysis of SAXS and dynamic and static multiangle light scattering data furthermore reveals that Ycg1 tends to oligomerize with increasing concentrations in the absence of Brn1. Based on these data, we present a model of the free Ycg1 protein constructed by normal mode analysis, as well as tentative models of Ycg1 dimers and tetramers. These models enable visualization of the conformational transitions that Ycg1 has to undergo to adopt a closed rigid shape and thereby create a DNA-binding surface in the condensin complex.

Condensins are protein complexes that play a key role during the segregation of eukaryotic chromosomes into the daughter cells during mitotic and meiotic cell divisions (1, 2). As members of the SMC (structural maintenance of chromosomes) family of complexes, they are thought to function by encircling chromosomal DNA within the large ring-shaped architecture that is created by a dimer of SMC subunits and a kleisin subunit (3–5). The Brn1^{Cnd2} kleisin subunit of condensin binds two additional subunits that are composed of tandem repeats of short, amphiphilic α-helices known as HEAT repeats (named after four proteins that contain this motif: Huntingtin, elongation factor 3, the A subunit of protein phosphatase 2A, and the signaling kinase TOR1) (6, 7).

Recent crystal structures of the *Saccharomyces cerevisiae* (*Sc*)[4] Ycg1 HEAT-repeat subunit in complex with the region of the Brn1 kleisin subunit it binds to and DNA revealed a positively charged groove that contacts the phosphate backbone of the dsDNA helix (8). In addition, DNA is entrapped within a flexible Brn1 loop, which thereby acts analogous to a safety belt that pins the DNA double helix in place. Interestingly, Ycg1 gains its ability to bind DNA only upon its association with the Brn1 subunit.

HEAT-repeat proteins have been shown to exhibit significant flexibility, both in response to binding events and as a result of external forces (9, 10). It therefore remains unclear whether the inability of Ycg1 to bind DNA by itself is merely due to the missing positive charges that are contributed by Brn1 residues and/or its safety-belt entrapment or whether binding to Brn1 induces structural transitions in the HEAT-repeat solenoid to create a DNA-binding site. The latter option would be analogous to the large conformational changes that other HEAT-repeat proteins undergo upon ligand binding (11, 12). Considering the essential function of the Ycg1–Brn1 DNA-binding site in recruiting condensin complexes to chromosomes (8, 13), it is essential to understand how DNA binding by Ycg1 is promoted upon its association with Brn1 and how this interaction is prevented when the protein is not assembled into condensin holocomplexes.

Here, we examined the structure and flexibility of the *Chaetomium thermophilum* (*Ct*) condensin subunit Ycg1 in solution using small-angle X-ray scattering (SAXS), both in its unbound form and in complex with the kleisin region Brn1$_{515-634}$ it binds to. Whereas the SAXS data confirmed the overall horseshoe-shaped Ycg1 conformation observed in the *Sc* Ycg1–Brn1 crystal structure, the unbound Ycg1 is considerably more flexible than the complex. This indicates that Brn1 binding significantly restricts the conformational freedom of Ycg1. Utilizing the high-resolution structure of *Sc* Ycg1–Brn1 as a starting point, we constructed models of monomeric *Ct* Ycg1 and the *Ct* Ycg1–Brn1$_{515-634}$ complex in solution by a normal mode analysis against the SAXS data.

This work was supported by German Research Foundation Grant HA 5853/2-1 (to C. H. H.) and by European Union Horizon 2020 Programme iNEXT Grant through Project 653706 (to D. I. S.) and European Research Council Consolidator Grant 681365 (to C. H. H.). The authors declare that they have no conflicts of interest with the contents of this article.

The data reported in this paper have been submitted to the Small Angle Scattering Biological Data Bank under accession nos. SASDFC4, SASDFD4, SASDFE4, SASDFF4, SASDFG4, SASDFH4, SASDFJ4, and SASDFK4.

[1] Candidate for joint Ph.D. degree from EMBL and Heidelberg University, Faculty of Biosciences.

[2] Present address: Dept. of Structural Biology, Genentech Inc., South San Francisco, CA 94080.

[3] To whom correspondence should be addressed: European Molecular Biology Laboratory, Hamburg Outstation, Hamburg 22607, Germany. E-mail: svergun@embl-hamburg.de.

[4] The abbreviations used are: *Sc*, *S. cerevisiae*; SAXS, small-angle X-ray scattering; NMA, normal mode analysis; *Ct*, *C. thermophilum*; SEC, size-exclusion chromatography; MALS, multiangle static light scattering; DLS, dynamic light scattering; MW, molecular weight; rmsd, root-mean-square deviation; CV, column volume; PDB, Protein Data Bank.

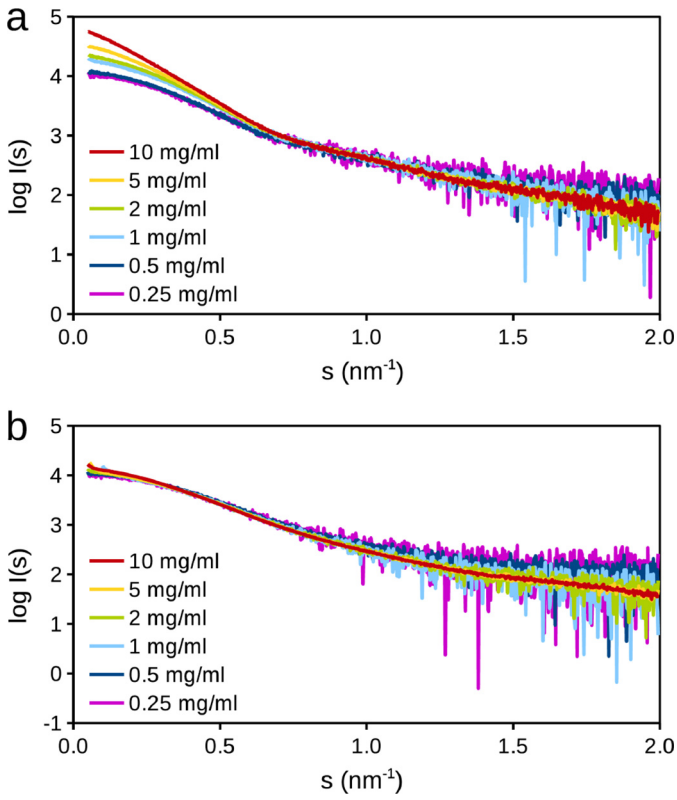

Figure 1. SAXS data collected for *Ct* Ycg1 reveal clear concentration-dependent oligomerization (*a*), whereas *Ct* Ycg1–Brn1 SAXS data show minimal unspecific aggregation instead (*b*).

We further found that Ycg1 assembly into condensin complexes prevents the protein from forming oligomers in solution. These findings have direct implications for the regulation of condensin function.

Results

To elucidate the solution structure of *Ct* Ycg1, both with and without the $Brn1_{515-634}$ fragment, SAXS data were collected for both samples at a series of concentrations. The processed scattering intensities after background subtraction are presented in Fig. 1 as functions of the momentum transfer $I(s)$, $s = 4\pi\sin\theta/\lambda$, where λ is the X-ray wavelength, and 2θ is the scattering angle. For Ycg1 alone, the normalized forward scattering, $I(0)$, and the apparent particle radius of gyration, R_g, significantly increase with the solute concentration, which indicates that the protein oligomerizes at higher concentrations (Fig. 1*a*). In sharp contrast, no obvious concentration dependence was observed for Ycg1–$Brn1_{515-634}$ except for minor unspecific aggregation effects (Fig. 1*b*).

The concentration series SAXS data for Ycg1 were used to extrapolate a scattering curve to apparent zero solute concentration, whereas Ycg1–$Brn1_{515-634}$ SAXS data were derived from merging low and high-concentration scattering data (see "Experimental procedures" for details). *Panels a* and *b* of Fig. 2 show the Ycg1 extrapolated data and the Ycg1–$Brn1_{515-634}$ merged data, with plots of their respective Guinier regions in the *lower left insets*. Both Ycg1 extrapolated data and the Ycg1–$Brn1_{515-634}$ merged data have linear Guinier regions, which indicates a lack of aggregation for both samples. The overall parameters computed from the scattering data are summarized in Table 1. The molecular weight (MW) estimates from the forward scattering, $I(0)$, for unbound Ycg1 and Ycg1–$Brn1_{515-634}$ confirm that the extrapolated and merged data represent monomeric forms in both cases. The pair distance distribution functions, $P(r)$, show that unbound Ycg1 appears slightly larger in solution than the Brn1-bound form (Fig. 2*c*), pointing to an increased Ycg1 flexibility in the absence of Brn1. The normalized Kratky plots for Ycg1 and Ycg1–$Brn1_{515-634}$ (Fig. 2*d*) furthermore suggest that unbound Ycg1 exhibits more flexibility than the Ycg1–$Brn1_{515-634}$ complex. Indeed, the latter plot is bell-shaped, which is characteristic of globular proteins, whereas the unbound protein reveals elevated scattering at higher angles, pointing to a higher anisometry/flexibility.

We reconstructed *ab initio* models of Ycg1 and Ycg1–$Brn1_{515-634}$ from the derived scattering curves of the two samples using DAMMIF (14). The resulting Ycg1 bead models are more extended than Ycg1–$Brn1_{515-634}$ bead models (Fig. 3, *a* and *b*), which also indicates that Brn1 binding restricts the flexibility of the Ycg1 HEAT-repeat solenoid.

The χ^2 fits between the Ycg1 and Ycg1–$Brn1_{515-634}$ SAXS data and the scattering profiles computed from their corresponding high-resolution structures are displayed in Fig. 2 (*a* and *b*). The scattering curve computed from the *Sc* Ycg1–Brn1 crystal structure yielded an overall good agreement with the *Ct* Ycg1–$Brn1_{515-634}$ SAXS data ($\chi^2 = 1.5$), whereas the scattering curve computed from the *Sc* Ycg1 component of the crystal structure alone showed noticeable systematic deviations against the unbound *Ct* Ycg1 SAXS data ($\chi^2 = 1.8$). To generate meaningful models that yield better fits, we performed SAXS-guided normal mode analysis (NMA). NMA starts with a high-resolution structure and fits the given scattering profile, allowing for larger-scale domain movements, as defined by harmonic normal modes (15). With this approach, it is possible to test whether allowing for a limited flexibility of the structure is sufficient to reconcile the models with the observed scattering data.

Fig. 3 (*c* and *d*) display the models of *Ct* Ycg1 and *Ct* Ycg1–$Brn1_{515-634}$ derived from SAXS-guided NMA. The Ycg1–$Brn1_{515-634}$ NMA model deviates from the crystal structure by 7 Å (rmsd), displaying essentially no differences at low resolution. In contrast, the Ycg1 NMA model is significantly more open and differs notably from the Ycg1 conformation in the Ycg1–Brn1 crystal structure (~17 Å rmsd). Because the unbound Ycg1 appears to be flexible, it might adopt multiple conformations in solution, and the obtained NMA model might therefore represent an average of these conformers, which clearly differ from the Brn1-bound Ycg1 in the crystal.

Given the observed concentration-dependent Ycg1 oligomerization in solution (Fig. 1*a*), we further utilized the SAXS data in the entire concentration range from 0.25 to 10 mg/ml Ycg1 to structurally characterize this process using the Ycg1 NMA model as a tentative monomeric unit. At 2 mg/ml, the MW estimate from $I(0)$ indicated that the protein is largely dimeric ($MW_{I(0)} \approx 204$ kDa). The MW determinations at protein concentrations lower than 2 mg/ml indicated a mixture of monomers and dimers, with the latter fraction increasing with concentration. We therefore used SASREFMX (16) to model a

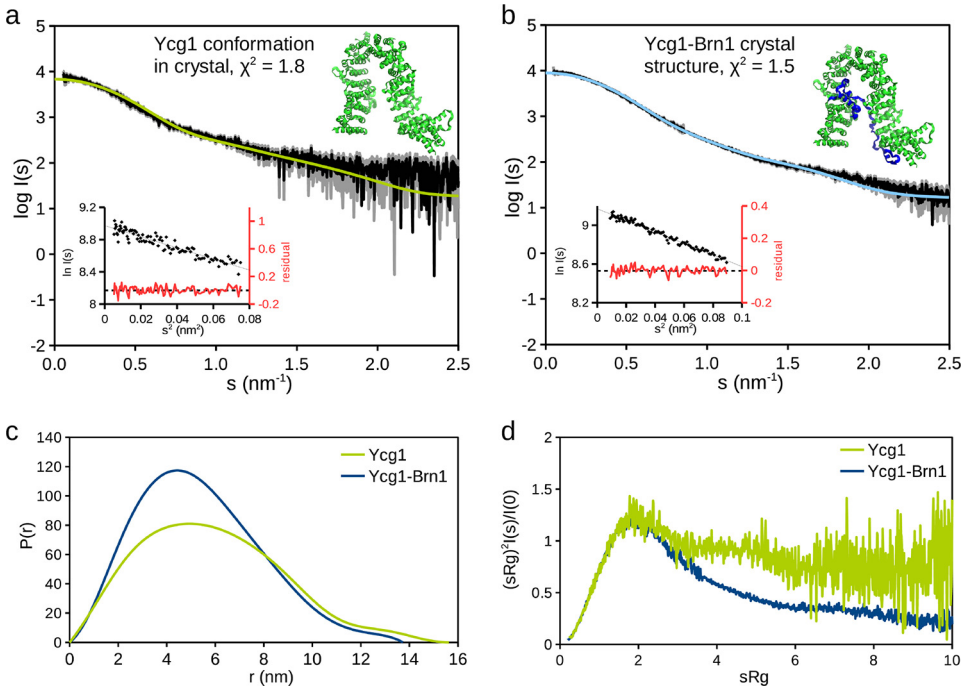

Figure 2. *a* and *b*, *Ct* Ycg1 extrapolated SAXS data (*a*), and *Ct* Ycg1–Brn1$_{515–634}$ merged SAXS data (*b*). For both *a* and *b*, the scattering curve computed for the high-resolution model is superimposed over the data. The Guinier plots are shown as *insets* on the *bottom left*, with the residuals shown in *red*. *c*, pair distance distributions computed from the scattering data for *Ct* Ycg1 and *Ct* Ycg1–Brn1$_{515–634}$ show differences in frequency of shorter distances, as well as maximum dimension. Unbound *Ct* Ycg1 appears slightly larger than the *Ct* Ycg1–Brn1$_{515–634}$ complex. *d*, normalized Kratky plots for *Ct* Ycg1 and *Ct* Ycg1–Brn1$_{515–634}$ data show that the Brn1-bound form is globular, whereas the unbound form exhibits more flexibility.

Table 1
Data collection and structure statistics for small angle X-ray scattering analysis

	Ycg1	Ycg1–Brn1$_{515–634}$
Data collection parameters		
Instrument	EMBL P12 (PETRA III, DESY, Hamburg, Germany)	EMBL P12 (PETRA III, DESY, Hamburg, Germany)
Beam geometry (mm^2)	0.2 × 0.12	0.2 × 0.12
Wavelength (Å)	1.24	1.24
s range (Å^{-1})	0.002–0.38	0.002–0.38
Exposure time (s)	1 (20 × 0.05 s)	1 (20 × 0.05 s)
Temperature (K)	283	283
Concentration range (mg ml^{-1})	0.25–10	0.25–10
Structural parameters		
R_g (Å) (from $P(r)$)	46 ± 1	42 ± 1
R_g (Å) (from Guinier plot)	46 ± 1	43 ± 1
D_{max} (Å)	160 ± 10	140 ± 10
Porod volume estimate (10^3 Å^3)	190	230
Excluded volume estimate (10^3 Å^3)[a]	186	205
Molecular mass determination (kDa)		
From Porod volume (V_p/~1.6)	119 ± 24	144 ± 29
From consensus Bayesian assessment (28)	109 ± 11	138 ± 15
From $I(0)$	102 ± 9	122 ± 10
Calculated monomeric molecular mass from sequence	109	125
Software employed		
Primary data reduction	SASFLOW	SASFLOW
Data processing	PRIMUS	PRIMUS
Ab initio analysis	DAMMIF	DAMMIF
Validation and averaging	DAMAVER	DAMAVER
Rigid body modelling	SASREFMX	NA[b]
Flexibility modeling	SREFLEX	SREFLEX
Computation of model intensities	CRYSOL	CRYSOL
3D graphics representations	PyMOL[c]	PyMOL[c]

[a] Excluded volume calculations made with the crystal structures, using Mol_volume, version 1.0, Theoretical Biophysics Group, University of Illinois (retrieved from http://www.ks.uiuc.edu/Development/MDTools/molvolume/; please note that the JBC is not responsible for the long-term archiving and maintenance of this site or any other third party hosted site).
[b] NA, not available.
[c] The PyMOL Molecular Graphics System, version 1.7.2.1, Schrödinger, LLC.

tentative dimeric structure and calculate the monomer-to-dimer ratio by simultaneous fitting of the entire set of SAXS data from 0.25 to 2 mg/ml. The obtained dimeric model is displayed in Fig. 4, along with the volume fractions of the dimer at different protein concentrations. In this model, the Ycg1 dimerization interface partially overlaps with the Brn1-

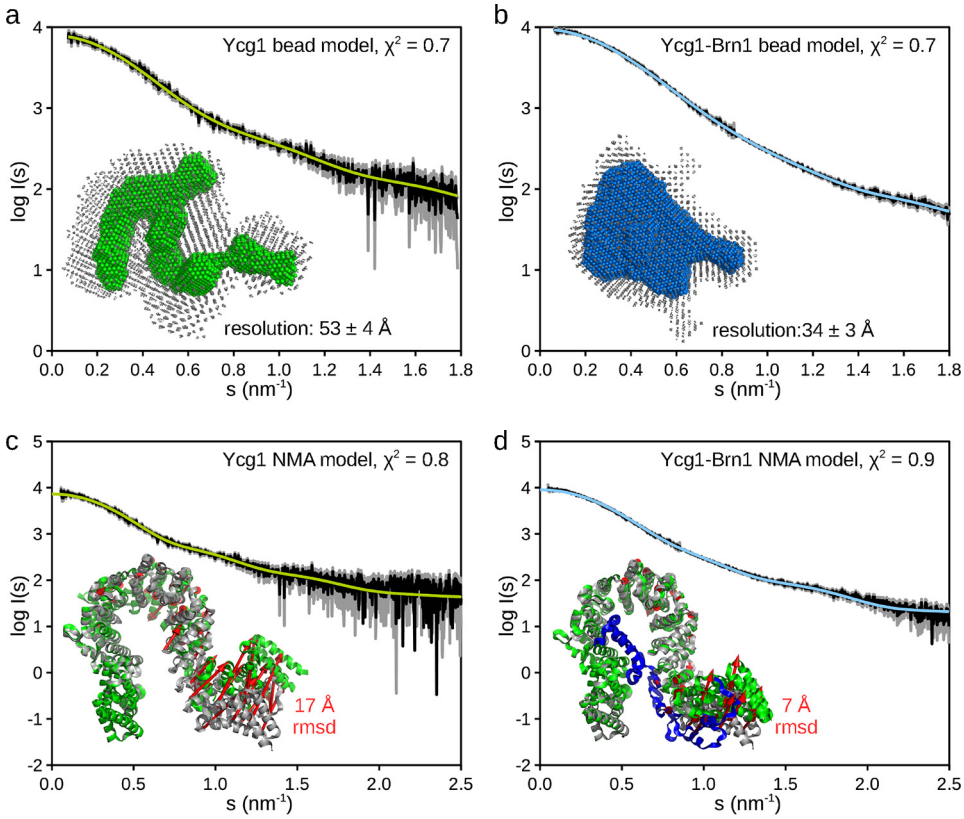

Figure 3. Modeling *Ct* Ycg1 and *Ct* Ycg1-Brn1$_{515-634}$ structures with SAXS data. *a* and *b*, *ab initio* models of *Ct* Ycg1 (*a*) and *Ct* Ycg1–Brn1$_{515-634}$ (*b*). For both *a* and *b*, a typical model is shown in the *lower left corner*, with the combined envelopes from 10 DAMMIF runs overlaid in *gray*. *Ct* Ycg1 bead models appear elongated compared with bead models of *Ct* Ycg1–Brn1$_{515-634}$. *c* and *d*, typical models of *Ct* Ycg1 (*c*) and *Ct* Ycg1–Brn1$_{515-634}$ (*d*) from normal mode analysis show similar features to the bead models. Initial Ycg1 structures are shown in *gray*, with the Brn1$_{515-634}$ peptide shown in *blue*. Ycg1 structures after NMA are shown in *green*. *Red arrows* on the initial structures depict the movement of the domains after NMA, with the net movement in angstroms displayed alongside. *Ct* Ycg1 has a much larger rmsd (17 Å) than *Ct* Ycg1–Brn1$_{515-634}$ (7 Å), which could be attributed to an increased flexibility in the absence of the ligand. For *a–d*, the scattering curves computed for the models (*smooth lines*) are superimposed on the scattering data (*black lines*).

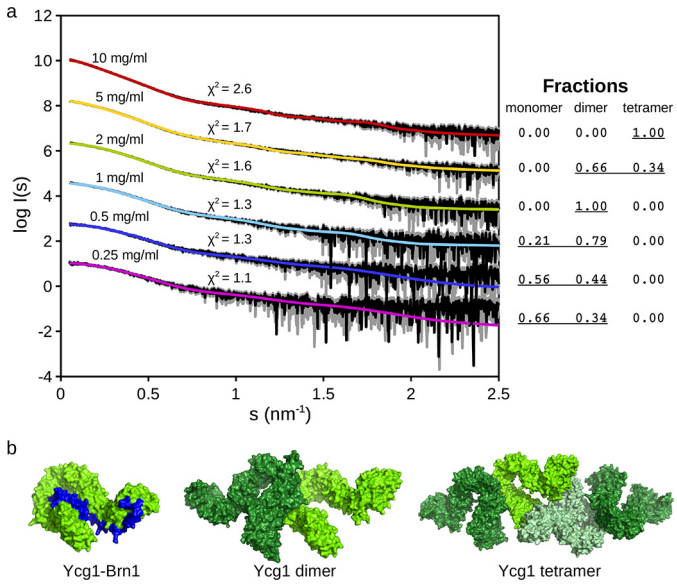

Figure 4. Ct Ycg1 concentration-dependent oligomerization. *a*, scattering data from a *Ct* Ycg1 concentration series were modeled as mixtures of monomer, dimer, and tetramer molecules. As *Ct* Ycg1 concentration increases, the amount of dimeric and tetrameric species in solution increases. *b*, the Ycg1–Brn1 crystal structure, compared with dimer and tetramer Ycg1 models. In the dimer model, the dimerization interface partly overlaps with the Brn1 (*blue*) binding site, which might explain why oligomerization was not observed to occur for *Ct* Ycg1–Brn1$_{515-634}$. The tetramer was built as a dimer of dimers.

binding site, which might also explain the lack of oligomerization in the Ycg1–Brn1$_{515-634}$ sample at comparable concentrations (Fig. 1*b*).

We further employed SASREFMX to follow the oligomerization of Ycg1 at yet higher concentrations (5 and 10 mg/ml). The analysis of possible higher-order oligomers indicated that the scattering data at 10 mg/ml can be well-represented by a tetramer, formed as a dimer of the Ycg1 dimer (Fig. 4*b*).

We validated the presence of higher oligomers of Ycg1 in solution using light scattering experiments. The dynamic light scattering (DLS) measurements revealed a systematic increase in the average hydrodynamic radius, R_h (from ~6.5 to ~9 nm), and apparent MW (from ~250 to ~500 kDa) with increasing solute concentration (Fig. 5*a*). Because the MW values deduced from DLS are dependent on the particle/oligomer shapes, which allows only a qualitative comparison, we complemented these data with a more quantitative method. Size-exclusion chromatography coupled to multiangle static light scattering (SEC–MALS) revealed three components in the elution profile. These components (marked with *arrows* in Fig. 5*b*) correspond to MW values of monomeric, dimeric and tetrameric Ycg1 (~100, ~200, and ~400 kDa). Both DLS and SEC–MALS results are in excellent agreement with the SAXS data and suggest a concentration-dependent oligomerization of Ycg1. The

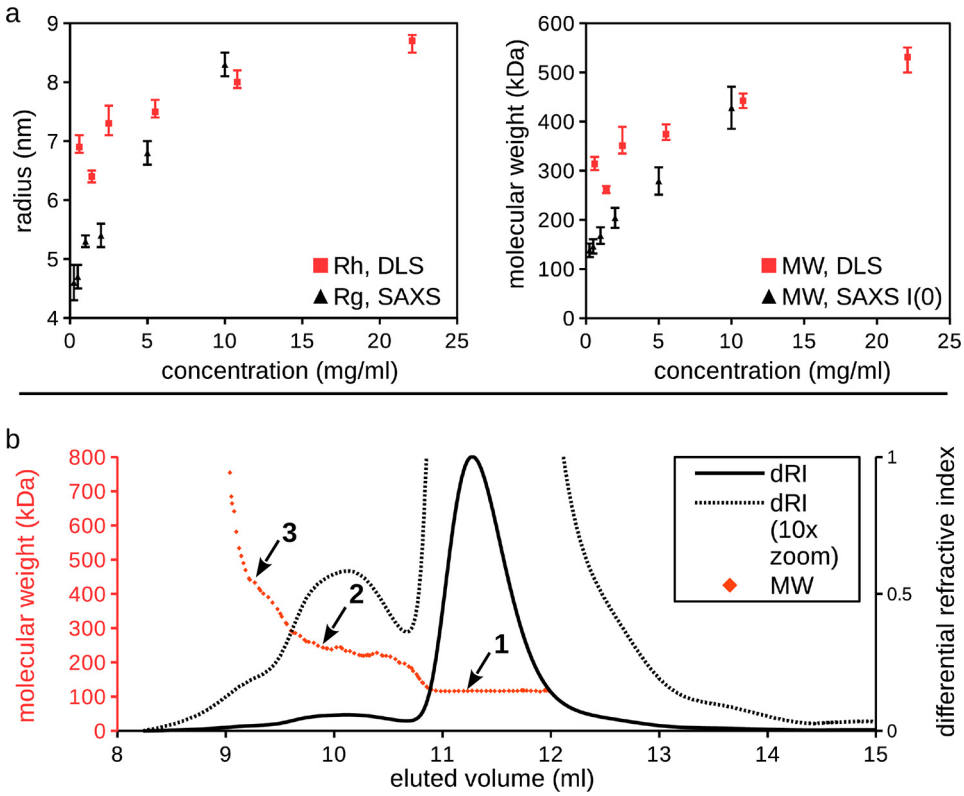

Figure 5. Concentration-dependent oligomerization of Ycg1 assessed by light scattering. *a*, batch DLS measurements show R_h and MW increasing with concentration, similar to SAXS. *b*, SEC–MALS of *Ct* Ycg1 confirms the presence of oligomeric species with monomeric (*arrow 1*, ~100 kDa), dimeric (*arrow 2*, ~200 kDa), and tetrameric (*arrow 3*, ~400 kDa) MWs. Note that the dimers and tetramers may be dissociating during chromatography because of dilution, causing them to be present in much smaller amounts compared with the SAXS experiment.

biological implications of this oligomerization are discussed below.

Discussion

By assembling into a complex with the kleisin subunit Brn1, the HEAT-repeat subunit Ycg1 forms the major DNA-binding site of the condensin complex and thereby controls the recruitment of condensin to chromosomes (8). It has been suggested that this recruitment triggers the subsequent ATP-dependent entrapment of DNA strands within the lumen of the large ring structure created by the SMC and kleisin subunits of condensin. Remarkably, the protein levels of budding yeast Ycg1 are strictly controlled by cell cycle–dependent transcription and protein degradation, which suggests that this subunit is the limiting factor for condensin holocomplex formation (17). It therefore seems conceivable that premature binding to chromosomes of Ycg1 molecules that have not yet assembled into condensin complexes needs to be prevented to achieve a controlled recruitment of condensin holocomplexes to chromosomes.

We found that the binding to Brn1 significantly restricts the flexibility of Ycg1 and converts an open and flexible configuration of free Ycg1 in solution, which is presumably facilitated by the elasticity of the HEAT-repeat architecture, into the horseshoe-shaped structure observed in crystal structures. A recent study on the human analog of the Ycg1–Brn1$_{515-634}$ complex suggests a similar modulation of the flexibility of the HEAT-repeat subunit by the binding of the kleisin (18). The crystal structure of this complex revealed a less tight interaction of the kleisin subunit than the one observed in the yeast Ycg1–Brn1 crystal structure and a more open conformation and greater flexibility (higher b-factors) of the HEAT-repeat subunit.

Flexibility of the unbound Ycg1 might be an essential prerequisite for its movement through the crowded cellular space (19) and for its assembly into condensin complexes. The SAXS data of free Ycg1 can be best fitted by a model that incorporates a large rotation of the N-terminal part of the HEAT-repeat solenoid (Fig. 3*c*). Remarkably, this is also the region of the protein that considerably contributes to the formation of the positively charged DNA-binding groove (8). These results strongly suggest that Brn1 binding promotes a structural transition in Ycg1, leading to a conformation that is amenable for making contacts with the phosphate backbone of the DNA double helix.

Fig. 6 shows a comparison between the *Sc* Ycg1–Brn1-DNA crystal structure and the SAXS-based NMA model of unbound *Ct* Ycg1. In the crystal structure, Brn1 contributes positively charged residues to the DNA-binding interface and directs positively charged residues located in the N and C termini of Ycg1 into a compact cluster amenable to DNA binding.

Although the condensin HEAT-repeat subunits have been speculated to self-assemble ("phase separate") via multivalent, weak interactions (19), no direct experimental evidence has yet supported this notion. The scattering data from Ycg1 strongly suggest that the higher MW species formed with increasing solute concentrations are specific oligomers rather than unspe-

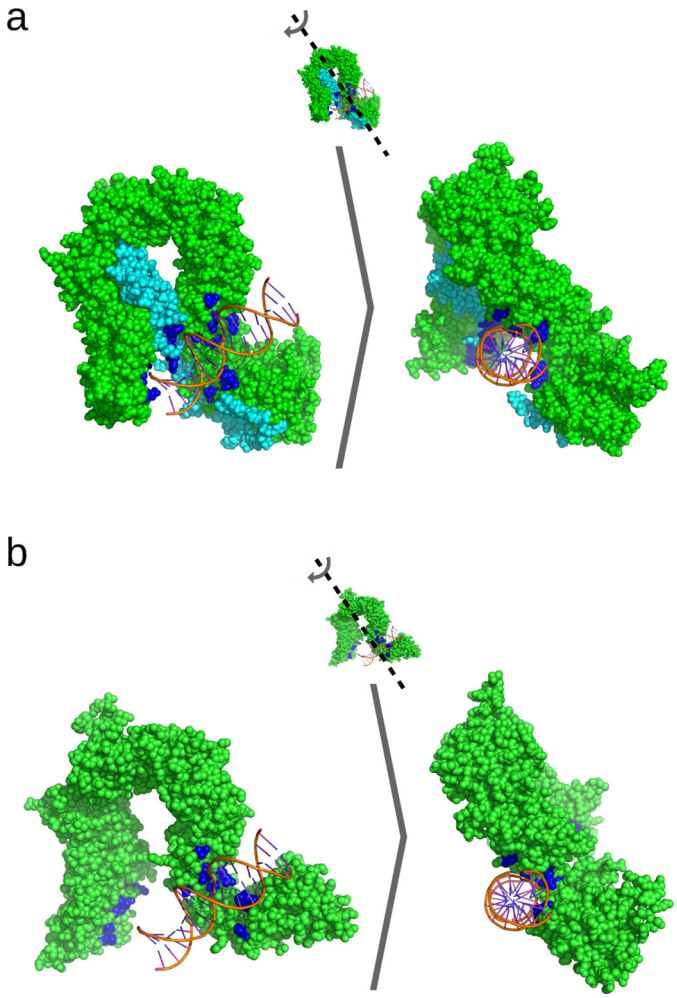

Figure 6. Comparison of Ycg1 conformation in the *Sc* Ycg1–Brn1-DNA crystal structure (PDB code 5OQP, *a*) and modeled with NMA to fit the monomeric *Ct* Ycg1 SAXS data (DNA superimposed for illustration purposes, *b*). Ycg1 is shown in *green*, and Brn1 is in *cyan*. In the crystal structure, Ycg1 and Brn1 form a DNA-binding interface with positively charged residues (shown in *blue*) from Brn1 and the N and C termini of Ycg1. In the absence of Brn1, Ycg1 was modeled with NMA to have a more open conformation, preventing the formation of the compact cluster of positive charges seen in Brn1-bound Ycg1.

cific aggregates. Indeed, the latter would not have yielded bell-shaped scattering curves, like the ones shown in Fig. 1*a*, and the scattering data from unspecific aggregates would also not be amenable to meaningful analyses in terms of oligomeric mixtures. The independent light scattering experiments (DLS and SEC–MALS) fully confirm the oligomerization observed by SAXS.

Future experiments will have to clarify the functional relevance of the observed oligomeric equilibria for Ycg1 and possibly for other HEAT-repeat proteins. However, already at this stage, our results further explain the finding that only the Ycg1–$Brn1_{515-634}$ complex, but not Ycg1 alone, is able to stably bind to DNA. Indeed, the observed dimerization of Ycg1 would probably not allow DNA binding and could thereby be part of the regulatory mechanism to prevent association of free Ycg1 molecules with chromatin. Furthermore, because the Brn1-binding site on Ycg1 overlaps with the Ycg1 dimerization interface (Fig. 4*b*), Brn1 binding might also dissociate the Ycg1 dimers to consequently allow chromatin association of assembled condensin complexes.

Experimental procedures

Sample preparation

Ct Ycg1 and the *Ct* Ycg1–$Brn1_{515-634}$ complex were both purified as described previously (8). The protein properties, such as the positions of purification tags and extinction coefficients, are listed in Table 2. In brief, proteins were expressed in *Escherichia coli* Rosetta (DE3) pLysS (Merck) from pET-MCN (20) vectors in 2× TY medium for 18 h at 18 °C. The cells were lysed by sonication in lysis buffer (500 mM NaCl, 50 mM Tris-HCl, pH 7.5, 20 mM imidazole, 5 mM β-mercaptoethanol, containing complete protease inhibitors (Roche)) at 4 °C, and the lysate was cleared by a centrifugation step at 45,000 × g_{max}. The cleared lysate was loaded onto nickel–Sepharose 6 Fast Flow (GE Healthcare) and extensively washed with 30–40 column volumes (CVs) of lysis buffer. The proteins were eluted in 5–7 CV elution buffer (lysis buffer plus 300 mM imidazole), and the combined eluate was dialyzed in SEC buffer (300 mM NaCl, 25 mM Tris-HCl, pH 7.5, 1 mM DTT) overnight at 4 °C. The dialyzed eluate was diluted with low-salt buffer (100 mM NaCl, 25 mM Tris-HCl, pH 7.5, 1 mM DTT) to a final salt concentration of 150 mM NaCl and loaded onto a 6 ml-RESOURCE Q (GE Healthcare) anion-exchange column pre-equilibrated with low-salt buffer. The column was washed with 3–5 CV of low-salt buffer, and the proteins were eluted with a linear NaCl concentration gradient to 1 M in 60 ml. The peak fractions were combined and loaded onto a Superdex 200 26/60 size-exclusion chromatography column equilibrated in SEC buffer. The peak fractions were pooled and concentrated by ultrafiltration (Vivaspin 30,000 MWCO, Sartorius), and the proteins were frozen at 10 mg/ml in liquid N_2.

Small-angle X-ray scattering data collection and processing

SAXS data for *Ct* Ycg1 and the *Ct* Ycg1–$Brn1_{515-634}$ complex were collected at the SAXS Beamline P12 of the PETRA III storage ring (Deutsches Elektronen-Synchrotron, Hamburg, Germany) (21). The details of the data collection conditions are summarized in Table 1. The scattering data in the momentum transfer range $0.002 < s < 0.38$ Å^{-1} were collected with a PILATUS 2M pixel detector at a distance of 4.0 m from the sample. For each sample, solute concentrations ranging from 0.25 to 10 mg/ml were measured. The samples were loaded using an automatic sample changer, and the solute was constantly flown through the capillary during the X-ray exposure to minimize radiation damage. The two-dimensional pixel data from the detector were converted to one-dimensional scattering profiles using the automated pipeline SASFLOW, which performed radial averaging, outlier removal, data averaging, and buffer subtraction (22).

The analyses of the SAXS data were performed using the ATSAS 2.8 suite (23). The data at different concentrations were assessed for quality in terms of the absence of repulsive or attractive interactions and signal-to-noise ratio. Based on these criteria, a composite scattering profile for Ycg1–$Brn1_{515-634}$ was generated by merging the low-angle scattering at 0.5 mg/ml and high-angle scattering at 5 mg/ml. For Ycg1, noticeable con-

Table 2
Sample properties

	Ycg1	Ycg1–Brn1$_{515–634}$
Organism	*C. thermophilum*	*C. thermophilum*
Source (reference)	Kschonsak *et al.* (8)	Kschonsak *et al.* (8)
Protein name (residues in construct)	Ycg1$_{24–1006}$ (N-terminal His$_6$ tag)	Ycg1$_{24–1006}$ in complex with Brn1$_{515–634}$ (N-terminal His$_6$ tag)
Extinction coefficient (A_{280}, M^{-1} cm^{-1})	48,820	69,790
Solvent	300 mM NaCl, 25 mM Tris-HCl, pH 7.5, 1 mM DTT	300 mM NaCl, 25 mM Tris-HCl, pH 7.5, 1 mM DTT

centration effects were observed, and the scattering data from 0.25 and 0.5 mg/ml were extrapolated to zero concentration using Primus (24). The Ycg1–Brn1$_{515–634}$ merged data and the Ycg1 extrapolated data were used for all subsequent data analyses including shape determination and rigid body modeling.

The forward scattering, $I(0)$, and the radius of gyration, R_g, were obtained from the Guinier approximation (25), following the standard procedures (26). The distribution of pair distances $P(r)$ was computed using the inverse Fourier transformation method implemented in GNOM (27). From the $P(r)$ function, an alternative estimate of R_g and the maximum particle dimension D_{max} were obtained. MWs of Ycg1 and Ycg1–Brn1$_{515–634}$ in solution were assessed from the SAXS data with three methods: (*a*) using the forward scattering, $I(0)$ (comparing against a reference solution of bovine serum albumin); (*b*) from the excluded (Porod) volume, V_p (given that V_p in nm^3 is ~1.6 times the MW in kDa) (16); and (*c*) a consensus Bayesian MW assessment method (28).

Molecular weight assessment with light scattering

The oligomeric states of Ycg1 were analyzed by analytical SEC–MALS. SEC was performed using an Agilent 1260 Infinity II Bio-inert LC system and an analytical Superdex 200 10/300 GL column (GE Healthcare) equilibrated with the sample buffer (25 mM Tris, 300 mM NaCl, 1 mM DTT, pH 7.5) at 20 °C. Seven microliters of Ycg1 at 10 mg/ml was injected, with the experiment performed at a flow rate of 0.8 ml/min. Protein elution was detected by absorbance at 280 nm, and protein concentration was quantified with differential refractometry using an Optilab T-rEX detector (Wyatt). Light scattering data were measured with a miniDAWN TREOS multiangle light scattering detector (Wyatt). Molecular weights were computed from the concentration and light scattering data using the software ASTRA version 7.1.3.15 (Wyatt).

Batch DLS measurements were also performed for Ycg1 at concentrations 0.6, 1.4, 2.5, 5.5, 10.8, and 22.1 mg/ml with a DynaPro NanoStar DLS detector (Wyatt). Light scattering data collection and analysis was performed with the software DYNAMICS version 7.6.0 (Wyatt). For each concentration, ten 5-s acquisitions were performed.

Data analysis and structure modeling

For the two samples, the *ab initio* modeling program DAMMIF (14) was used to produce low-resolution bead models from the measured SAXS data. Because the structural modeling with SAXS data are potentially ambiguous, analysis of model variability and uniqueness was performed. Ten independent DAMMIF models were generated, superimposed with SUPCOMB (29), compared, and averaged using DAMAVER (30).

The theoretical scattering curves from the high-resolution models of *Sc* Ycg1 and Ycg1–Brn1 (PDB code 5OQQ) were computed, and their χ^2 fits against the experimental SAXS data evaluated using CRYSOL (31). The χ^2 fit is defined as follows,

$$\chi^2 = \frac{1}{N_p}\sum_{i=1}^{N_p}\left[\frac{I_e(s_i) - cI_m(s_i)}{\sigma(s_i)}\right]^2 \quad \text{(Eq. 1)}$$

where N_p is the number of experimental points, I_e is the experimental scattering, I_m is the computed scattering from the PDB model, $\sigma(s_i)$ is the experimental error, and c is the scaling factor.

To improve the χ^2 fits from the free *Sc* Ycg1 and from Ycg1–Brn1, the two high-resolution models were refined by NMA using the program SREFLEX (15). This program partitions the structure into pseudo-domains and hierarchically employs NMA to find the domain rearrangements minimizing the χ^2 between the SAXS curve computed from the refined model and the experimental data.

Because the unbound Ycg1 exhibited signs of oligomerization, a dimer structure and its proportion at elevated concentrations in solution was further modeled using SASREFMX (16). This program constructs dimeric models and fits a set of SAXS data measured at different concentrations by mixtures of the monomers and dimers in the mixture. The SAXS data for Ycg1 at $c = 5$ and 10 mg/ml were further modeled with SASREFMX as a mixture of monomers, dimers, and tetramers, with the tetrameric structure built as a dimer of dimers.

The experimental SAXS data described here, as well as the models derived from them, were deposited in the Small Angle Scattering Biological Data Bank under accession numbers SASDFC4 (Ycg1 monomer), SASDFD4 (Ycg1–Brn1 monomer), SASDFE4 (Ycg1 tetramer), SASDFG4 (Ycg1 dimer), and SASDFF4, SASDFH4, SASDFJ4, and SASDFK4 (Ycg1 concentration series) (32).

Author contributions—K. M.-C., M. K., C. H. H., and D. I. S. conceptualization; K. M.-C. and D. I. S. formal analysis; K. M.-C. and D. I. S. validation; K. M.-C. investigation; K. M.-C. visualization; K. M.-C. and M. K. methodology; K. M.-C. and M. K. writing-original draft; K. M.-C. and D. I. S. project administration; K. M.-C., M. K., C. H. H., and D. I. S. writing-review and editing; C. H. H. and D. I. S. resources; C. H. H. and D. I. S. supervision; C. H. H. and D. I. S. funding acquisition.

Acknowledgments—We are grateful to Melissa Graewert for assistance with the light scattering experiments and Markus Hassler for comments on the manuscript.

References

1. Houlard, M., Godwin, J., Metson, J., Lee, J., Hirano, T., and Nasmyth, K. (2015) Condensin confers the longitudinal rigidity of chromosomes. *Nat. Cell Biol.* **17,** 771–781 CrossRef Medline
2. Uhlmann, F. (2016) SMC complexes: from DNA to chromosomes. *Nat. Rev. Mol. Cell Biol.* **17,** 399–412 CrossRef
3. Cuylen, S., Metz, J., and Haering, C. H. (2011) Condensin structures chromosomal DNA through topological links. *Nat. Struct. Mol. Biol.* **18,** 894–901 CrossRef Medline
4. Ivanov, D., and Nasmyth, K. (2005) A topological interaction between cohesin rings and a circular minichromosome. *Cell* **122,** 849–860 CrossRef Medline
5. Wilhelm, L., Bürmann, F., Minnen, A., Shin, H. C., Toseland, C. P., Oh, B. H., and Gruber, S. (2015) SMC condensin entraps chromosomal DNA by an ATP hydrolysis dependent loading mechanism in *Bacillus subtilis*. *eLife* **4,** 06659 CrossRef Medline
6. Andrade, M. A., and Bork, P. (1995) HEAT repeats in the Huntington's disease protein. *Nat. Genet.* **11,** 115–116 CrossRef Medline
7. Neuwald, A. F., and Hirano, T. (2000) HEAT repeats associated with condensins, cohesins, and other complexes involved in chromosome-related functions. *Genome Res.* **10,** 1445–1452 CrossRef Medline
8. Kschonsak, M., Merkel, F., Bisht, S., Metz, J., Rybin, V., Hassler, M., and Haering, C. H. (2017) Structural basis for a safety-belt mechanism that anchors condensin to chromosomes. *Cell* **171,** 588–600.e24 CrossRef Medline
9. Grinthal, A., Adamovic, I., Weiner, B., Karplus, M., and Kleckner, N. (2010) PR65, the HEAT-repeat scaffold of phosphatase PP2A, is an elastic connector that links force and catalysis. *Proc. Natl. Acad. Sci. U.S.A.* **107,** 2467–2472 CrossRef Medline
10. Kappel, C., Zachariae, U., Dölker, N., and Grubmüller, H. (2010) An unusual hydrophobic core confers extreme flexibility to HEAT repeat proteins. *Biophys. J.* **99,** 1596–1603 CrossRef Medline
11. Fukuhara, N., Fernandez, E., Ebert, J., Conti, E., and Svergun, D. (2004) Conformational variability of nucleo-cytoplasmic transport factors. *J. Biol. Chem.* **279,** 2176–2181 CrossRef Medline
12. Forwood, J. K., Lange, A., Zachariae, U., Marfori, M., Preast, C., Grubmüller, H., Stewart, M., Corbett, A. H., and Kobe, B. (2010) Quantitative structural analysis of importin-β flexibility: paradigm for solenoid protein structures. *Structure* **18,** 1171–1183 CrossRef Medline
13. Piazza, I., Rutkowska, A., Ori, A., Walczak, M., Metz, J., Pelechano, V., Beck, M., and Haering, C. H. (2014) Association of condensin with chromosomes depends on DNA binding by its HEAT-repeat subunits. *Nat. Struct. Mol. Biol.* **21,** 560–568 CrossRef Medline
14. Franke, D., and Svergun, D. I. (2009) DAMMIF, a program for rapid *ab-initio* shape determination in small-angle scattering. *J. Appl. Crystallogr.* **42,** 342–346 CrossRef Medline
15. Panjkovich, A., and Svergun, D. I. (2016) Deciphering conformational transitions of proteins by small angle X-ray scattering and normal mode analysis. *Phys. Chem. Chem. Phys.* **18,** 5707–5719 CrossRef Medline
16. Petoukhov, M. V., Franke, D., Shkumatov, A. V., Tria, G., Kikhney, A. G., Gajda, M., Gorba, C., Mertens, H. D., Konarev, P. V., and Svergun, D. I. (2012) New developments in the ATSAS program package for small-angle scattering data analysis. *J. Appl. Crystallogr.* **45,** 342–350 CrossRef Medline
17. Doughty, T. W., Arsenault, H. E., and Benanti, J. A. (2016) Levels of Ycg1 limit condensin function during the cell cycle. *PLoS Genet.* **12,** e1006216 CrossRef Medline
18. Hara, K., Kinoshita, K., Migita, T., Murakami, K., Shimizu, K., Takeuchi, K., Hirano, T., and Hashimoto, H. (2019) Structural basis of HEAT–kleisin interactions in the human condensin I subcomplex. *EMBO Rep.* **20,** e47183 CrossRef Medline
19. Yoshimura, S. H., and Hirano, T. (2016) HEAT repeats: versatile arrays of amphiphilic helices working in crowded environments? *J. Cell Sci.* **129,** 3963–3970 Medline
20. Romier, C., Ben Jelloul, M., Albeck, S., Buchwald, G., Busso, D., Celie, P. H., Christodoulou, E., De Marco, V., van Gerwen, S., Knipscheer, P., Lebbink, J. H., Notenboom, V., Poterszman, A., Rochel, N., Cohen, S. X., *et al.* (2006) Co-expression of protein complexes in prokaryotic and eukaryotic hosts: experimental procedures, database tracking and case studies. *Acta Crystallogr. D Biol. Crystallogr.* **62,** 1232–1242 CrossRef Medline
21. Blanchet, C. E., Spilotros, A., Schwemmer, F., Graewert, M. A., Kikhney, A., Jeffries, C. M., Franke, D., Mark, D., Zengerle, R., Cipriani, F., Fiedler, S., Roessle, M., and Svergun, D. I. (2015) Versatile sample environments and automation for biological solution X-ray scattering experiments at the P12 beamline (PETRA III, DESY). *J. Appl. Crystallogr.* **48,** 431–443 CrossRef Medline
22. Franke, D., Kikhney, A. G., and Svergun, D. I. (2012) Automated acquisition and analysis of small angle x-ray scattering data. *Nucl. Instrum. Meth. A* **689,** 52–59 CrossRef
23. Franke, D., Petoukhov, M. V., Konarev, P. V., Panjkovich, A., Tuukkanen, A., Mertens, H. D., Kikhney, A. G., Hajizadeh, N. R., Franklin, J. M., Jeffries, C. M., and Svergun, D. I. (2017) ATSAS 2.8: A comprehensive data analysis suite for small-angle scattering from macromolecular solutions. *J. Appl. Crystallogr.* **50,** 1212–1225 CrossRef Medline
24. Konarev, P. V., Volkov, V. V., Sokolova, A. V., Koch, M. H., and Svergun, D. I. (2003) PRIMUS: a Windows PC-based system for small-angle scattering data analysis. *J. Appl. Crystallogr.* **36,** 1277–1282 CrossRef
25. Guinier, A. (1939) X-ray diffraction at very small angles: application to the study of ultramicroscopic phenomena. *Ann. Phys.* (*Paris*) **11,** 161–237 CrossRef
26. Petoukhov, M. V., Konarev, P. V., Kikhney, A. G., and Svergun, D. I. (2007) ATSAS 2.1: towards automated and web-supported small-angle scattering data analysis. *J. Appl. Crystallogr.* **40,** 223–228 CrossRef
27. Svergun, D. I. (1992) Determination of the regularization parameter in indirect-transform methods using perceptual criteria. *J. Appl. Crystallogr.* **25,** 495–503 CrossRef
28. Hajizadeh, N. R., Franke, D., Jeffries, C. M., and Svergun, D. I. (2018) Consensus Bayesian assessment of protein molecular mass from solution X-ray scattering data. *Sci. Rep.* **8,** 7204 CrossRef Medline
29. Kozin, M. B., and Svergun, D. I. (2001) Automated matching of high- and low-resolution structural models. *J. Appl. Crystallogr.* **34,** 33–41 CrossRef
30. Volkov, V. V., and Svergun, D. I. (2003) Uniqueness of *ab initio* shape determination in small-angle scattering. *J. Appl. Crystallogr.* **36,** 860–864 CrossRef
31. Svergun, D. I., Barberato, C., and Koch, M. H. J. (1995) CRYSOL: a program to evaluate X-ray solution scattering of biological macromolecules from atomic coordinates. *J. Appl. Crystallogr.* **28,** 768–773 CrossRef
32. Valentini, E., Kikhney, A. G., Previtali, G., Jeffries, C. M., and Svergun, D. I. (2015) SASBDB, a repository for biological small-angle scattering data. *Nucleic Acids Res.* **43,** D357–D363 Medline